TISSUE ENGINEERING: Part A
Volume 15, Number 8, 2009

DOI: 10.1089/ten.tea.2008.0433

Original Article

Comparative Evaluation of Nanofibrous Scaffolding for Bone Regeneration in Critical-Size Calvarial Defects

Kyung Mi Woo, D.D.S., Ph.D.,[1] Victor J. Chen, Ph.D.,[2] Hong-Moon Jung, B.S.,[1]
Tae-Il Kim, D.D.S., Ph.D.,[3] Hong-In Shin, D.D.S., Ph.D.,[4] Jeong-Hwa Baek, D.D.S., Ph.D.,[1]
Hyun-Mo Ryoo, D.D.S., Ph.D.,[1] and Peter X. Ma, Ph.D.[2,5,6]

In a previous study we found that nanofibrous poly(L-lactic acid) (PLLA) scaffolds mimicking collagen fibers in size were superior to solid-walled scaffolds in promoting osteoblast differentiation and bone formation *in vitro*. In this study we used an *in vivo* model to confirm the biological properties of nanofibrous PLLA scaffolds and to evaluate how effectively they support bone regeneration against solid-walled scaffolds. The scaffolds were implanted in critical-size defects made on rat calvarial bones. Compared with solid-walled scaffolds, nanofibrous scaffolds supported substantially more new bone tissue formation, which was confirmed by micro-computed tomography measurement and von Kossa staining. Goldner's trichrome staining showed abundant collagen deposition in nanofibrous scaffolds but not in the control solid-walled scaffolds. The cells in these scaffolds were immuno-stained strongly for Runx2 and bone sialoprotein (BSP). In contrast, solid-walled scaffolds implanted in the defects were stained weakly with trichrome, Runx2, and BSP. These *in vivo* results demonstrate that nanofibrous architecture enhances osteoblast differentiation and bone formation.

Introduction

Scaffolds play a critical role in tissue engineering, which aims to regenerate missing tissues or organs.[1] Because they serve as artificial temporary extracellular matrix (ECM) until cells replace them with newly synthesized natural ECM, scaffolds should reproduce the structural and biochemical functions of natural ECM. The performance of a scaffold is affected by several factors, including the chemical nature of the scaffolding material and the physical structures at various size scales, which are dependent on the method of fabrication. It is often beneficial for the scaffolds to mimic certain advantageous characteristics of the natural ECM, or developmental or wound healing programs.[2]

Because natural ECM is mainly composed of fibrous collagen, our laboratory and others have proposed to develop nanofibrous materials as advanced scaffolds for tissue engineering.[3–5] Various techniques, including electrospinning,[6–8] self-assembly,[9,10] and phase separation,[3,4,11–13] have recently been explored to fabricate nanofibrous materials. Our laboratory has developed a novel phase separation method to generate synthetic nanofibrous scaffolds with a morphology similar to that of natural collagen fibers, unique in that it allows for the design of pore structure.[2] While there has been active development of the nanofibrous scaffolds, there are limited comparative reports providing evidence that nanofibrous scaffolds are superior to conventional solid-walled scaffolds.[14–16] Previously, we reported that, compared with solid-walled scaffolds, nanofibrous scaffolds improved adsorption of proteins, including fibronectin and vitronectin, both of which may mediate cell interactions with the scaffold.[15] The nanofibrous and solid-walled scaffolds were made from the same biodegradable polymer, poly(L-lactic acid) (PLLA), and have similar macropore structure (interconnected spherical pores formed by paraffin sphere porogen, pore diameter = 250–420 μm).[15] Both the nanofibrous (average fiber diameter was between 100 and 200 nm) and solid-walled scaffolds had similar porosities of 96% (calculated from scaffold mass, dimensions, and crystallinity).[15] The only difference was in the wall architecture of the macropores. Special processing conditions were employed to form the macropores of the nanofibrous scaffolds, as previously published.[4,11,17] Using an *in vitro* culture system, we found that synthetic nanofibers (mimicking the geometrical

[1]Department of Cell & Developmental Biology, Dental Research Institute and BK21 Program, School of Dentistry, Seoul National University, Seoul, Republic of Korea.
[2]Department of Biomedical Engineering, University of Michigan, Ann Arbor, Michigan.
[3]Department of Periodontology, School of Dentistry, Seoul National University, Seoul, Republic of Korea.
[4]Department of Oral Pathology, School of Dentistry, Kyungpook National University, Taegu, Republic of Korea.
[5]Department of Biologic and Materials Sciences, University of Michigan, Ann Arbor, Michigan.
[6]Macromolecular Science and Engineering Center, University of Michigan, Ann Arbor, Michigan.

features of collagen fibers) advantageously support osteoblastic differentiation and biomineralization.[16,18] In the present study, we evaluated the 3D nanofibrous scaffolds on *in vivo* bone formation in comparison to 3D solid-walled scaffolds. Critical-size defects were made at the center of calvarial bone in rats. Scaffolds without cells were implanted in the defects. Bone formation in the defects was evaluated using micro-computed tomography (micro-CT) and von Kossa staining. Formation of collagen fibers was examined by Goldner's trichrome staining. Osteoblastic differentiation of cells in scaffolds was examined through immunostaining for Runx2 and bone sialoprotein (BSP). The results suggest that the nanofibrous morphology of the scaffolds promotes osteoblast differentiation and bone formation *in vivo*.

Materials and Methods

Preparation of nanofibrous and solid-walled PLLA scaffolds

The scaffold preparation has been reported in detail previously.[11,15] Briefly, for nanofibrous PLLA scaffolds, a 12.5% (w/v) PLLA solution in a 1:1 (v/v) mixture of dioxane and pyridine, was prepared by stirring at 60°C for 1–2 h until a homogeneous solution was obtained. Paraffin spheres (diameter, 250–420 μm; 0.40 ± 0.01 g) were added to Teflon molds, and heat-treated at 37°C for 45 min. After the molds were cooled to room temperature, prepared polymer solution (0.32 mL) was added dropwise onto each paraffin sphere assembly, and the assembly was treated in a vacuum oven (250 mmHg, ~37°C) to remove air trapped inside the paraffin sphere assemblies. Vacuum treatment was done as quickly as possible to avoid further bonding of the paraffin spheres. The polymer solution was induced to phase-separate at −70°C overnight. The molds were then immersed into cold hexane for 2 days (−18°C) to extract the solvent. The materials were removed from the molds and punched into disks 8 mm in diameter and 1.5 mm in thickness. The specimens were then placed into hexane to extract the remaining solvent and to leach the paraffin. Specimens were kept in hexane at room temperature for 2 days, and the hexane was changed three times every day. Hexane was then replaced with cyclohexane, and the polymer matrices were removed from the cyclohexane and frozen at −70°C for at least 6 h. The frozen matrices were then lyophilized at −70°C, placed under vacuum (<30 mmHg) for 7 days, placed in an ice/salt bath (−5 to −10°C, <30 mmHg) for two additional days, and dried at room temperature under the same pressure for the final 2 days.

For PLLA solid-walled scaffolds, a 12.5% (w/v) PLLA solution was prepared by stirring in dioxane at 60°C for 1–2 h until a homogeneous solution was obtained. The paraffin sphere mold preparation and the polymer casting procedures were performed in the same manner as for the nanofibrous scaffolds. After polymer solution casting, the polymer/paraffin composites were dried under low vacuum (≈340 mmHg) overnight, and under high vacuum (<30 mmHg) for four additional days. Samples were removed from the molds and punched into disks 8 mm in diameter and 1.5 mm in thickness. Paraffin leaching with hexane, solvent exchange with cyclohexane, and lyophilizing procedures were performed in the same manner as for the nanofibrous scaffolds. The nanofibrous and solid-walled scaffolds were sterilized with ethylene oxide following the manufacturer's procedure (H.W. Anderson Products, Chapel Hill, NC).

Animals and surgical procedures

All procedures were approved by Institute of Laboratory Animal Resources at Seoul National University (authorization number SNU-050608-3). Sprague–Dawley rats (250–300 g) were used in this study. Sample size was determined as $n = 4$, based on the pilot result of micro-CT [$\alpha = 0.05$, $\beta = 0.20$, and $\sigma = 1.1$; effect size (expected mean difference in the newly formed bone volume) = 2.2]. A critical-size rat calvarial bone defect was created as previously described.[19] The animals were anesthetized with a subcutaneous injection of a mixture of ketamine and xylazine (40 and 9 mg/kg, respectively). The scalp covering the calvarial vault was shaved and scrubbed with betadine solution and infiltrated with a local anesthetic agent of 2% lidocaine with 1:100,000 epinephrine. An incision was made along the midline. Full-thickness skin and the periosteum were raised to expose the calvarial bone surface. Careful drilling with an 8-mm-diameter trephine bur was done around the sagittal suture, and a standardized, round, segmental defect was made. During drilling, the area was irrigated with saline solution and the underlying dura mater was maintained intact. A nanofibrous or a solid-walled scaffold, without cells, was placed in the defect. The periosteum (pericranium) and skin were closed in layers with absorbable 5–0 chromic catgut (WRHI, Namyangju, Korea) and nonabsorbable 4–0 black silk (Ethicon, Edinburgh, United Kingdom) sutures, respectively.

Micro-CT

Rats were sacrificed 4 or 8 weeks after scaffold implantation. Calvarial bone was excised, trimmed, and fixed in 4% paraformaldehyde for 24 h at 4°C. The specimens were examined using a micro-CT machine (Skyscan 1072; Skyscan, Aartselaar, Belgium). Specimens were placed on a cylindrical sample holder with the coronal aspect of calvarial bone in a horizontal position to ensure parallel scanning conditions. The resolution was set at 19.5 μm, averaging by two frames with median filtration. Rotation step of 0.9° and rotation angle of 180° were set to take approximately 500 slices of the scan. Files were reconstructed using a modified Feldkamp algorithm, which was created using microtomographic analysis software (TomoNT; Skyscan). After the 3D visualizing process, bone volumes were measured in the region of interest from four animals in each group. In addition, micro-CT scan was also performed in animals of which defects were not treated with any scaffolds, serving as the negative control. The bone volume was obtained by subtracting the value of negative control from the value of the experimental specimen. The data are presented as average ± standard error of means (SEM). Student's *t*-test was done using Microsoft Excel software to compare the differences between two groups.

Histology

After micro-CT measurement, the specimen was divided into two parts along the sagittal suture for the calcified and decalcified section preparations. The specimens for the cal-

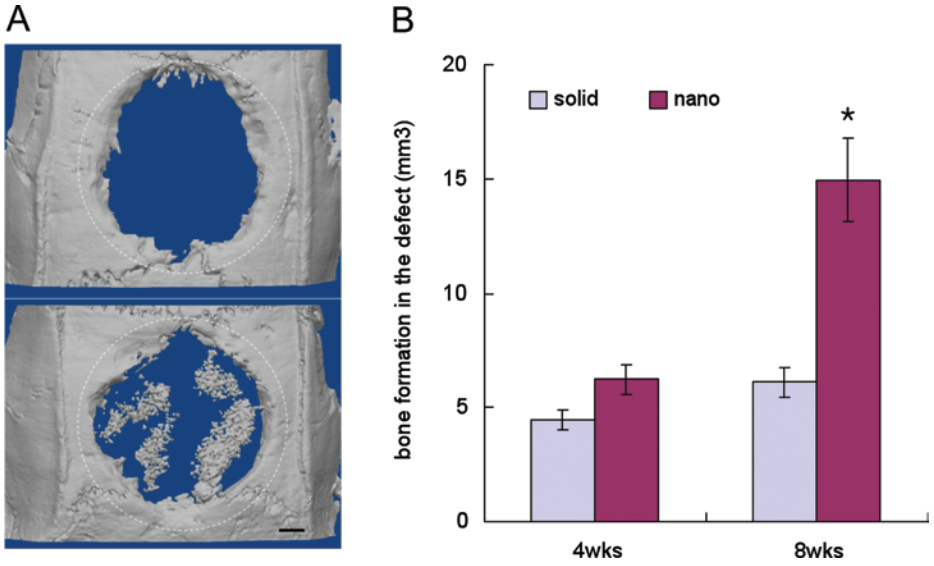

FIG. 1. Bone formation in rat critical-size calvarial defects. (**A**) Reconstructed micro-CT images of the scaffolds implanted for 8 weeks (upper, solid-walled scaffolds; lower, nanofibrous scaffolds). The dotted circles indicate the original defect. Bar length: 1 mm. (**B**) Bone volumes of the constructs after subtracting the value of the negative control (not treated with any scaffold). Data are presented as average ± SEM. ($n = 4$). *Statistically significant (Student's t-test, $p < 0.05$). Color images available online at www.liebertonline.com/ten.

cified section were placed in 70% ethanol, dehydrated in graded concentrations of alcohol, and embedded in methymethacrylate resin (Technovit® 9100; Kulzer, Wehrheim, Germany). After the resin blocks were trimmed, 5-μm-thick sections were prepared with a microtome (Leica RM2156; Leica, Wetzlar, Germany) equipped with a tungsten carbide knife. The sections were stained with von Kossa and Goldner's trichrome. The samples for the decalcified section were decalcified in 10% EDTA for 10 days at room temperature, dehydrated through ascending graded alcohol, embedded in paraffin, sectioned at 5 μm, and stained with H&E.

Immunostaining

Immunostaining was performed for Runx2 and BSP. The sections from four animals in each group were deparaffinized, washed in PBS, and heated in a microwave for 2 min. The sections were incubated in a 3% H_2O_2 solution to quench any endogenous peroxidases in the section. The sections were blocked with 1% antigoat serum in PBS for 30 min at room temperature, and incubated in primary anti-Runx2 antibody (Santa Cruz Biotechnology, Santa Cruz, CA) or anti-BSP antibody (developed by Solursh and Franzen, obtained from the Developmental Studies Hybridoma Bank under the auspices of the NICHD and maintained at The University of Iowa in the Department of Biological Sciences) at 4°C overnight. Incubation in the isotype-control antibodies (antirabbit IgG for Runx2, antimouse IgG_2 for BSP; Santa Cruz Biotechnology) was also performed and served as negative controls of immunostaining. After washing with PBS, the sections were incubated in horseradish peroxidase–conjugated secondary antibodies for 30 min at room temperature, followed

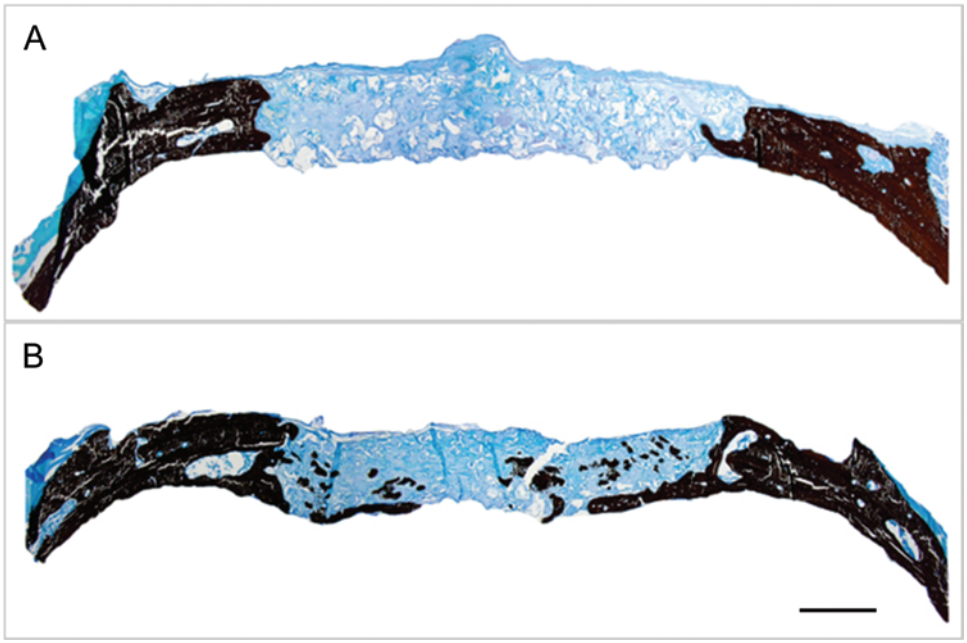

FIG. 2. Von Kossa staining views of scaffolds implanted in calvarial defects for 8 weeks. (**A**) Solid-walled scaffolds; (**B**) nanofibrous scaffolds. Original magnification, 20 ×. Bar length: 1 mm. Representative images are presented. Color images available online at www.liebertonline.com/ten.

by treatment with diaminobenzidene solution (DAB; Dako Cytomation, Carpinteria, CA).

Results

Bone formation in the calvarial defects

Bone formation was evident in the nanofibrous scaffolds implanted in critical-size calvarial bone defects. This observation was confirmed by micro-CT measurements and von Kossa staining (Figs. 1 and 2). New bone formation in the bony defects measured by micro-CT 8 weeks after implantation was about 2.1-fold higher in the nanofibrous scaffolds than in the solid-walled scaffolds (Fig. 1), obtained by subtracting the bone volume of negative controls from that of the experimental constructs (Fig. 1B). At an earlier time point of 4 weeks after implantation, the difference between the two scaffold groups in bone volume was not statistically significant; only one out of four nanofibrous scaffolds contained noticeable amounts of newly formed bone tissue at that time (data not shown). However, at 8 weeks after implantation, significantly more bone formation in the nanofibrous scaffolds than in the solid-walled scaffolds was consistently

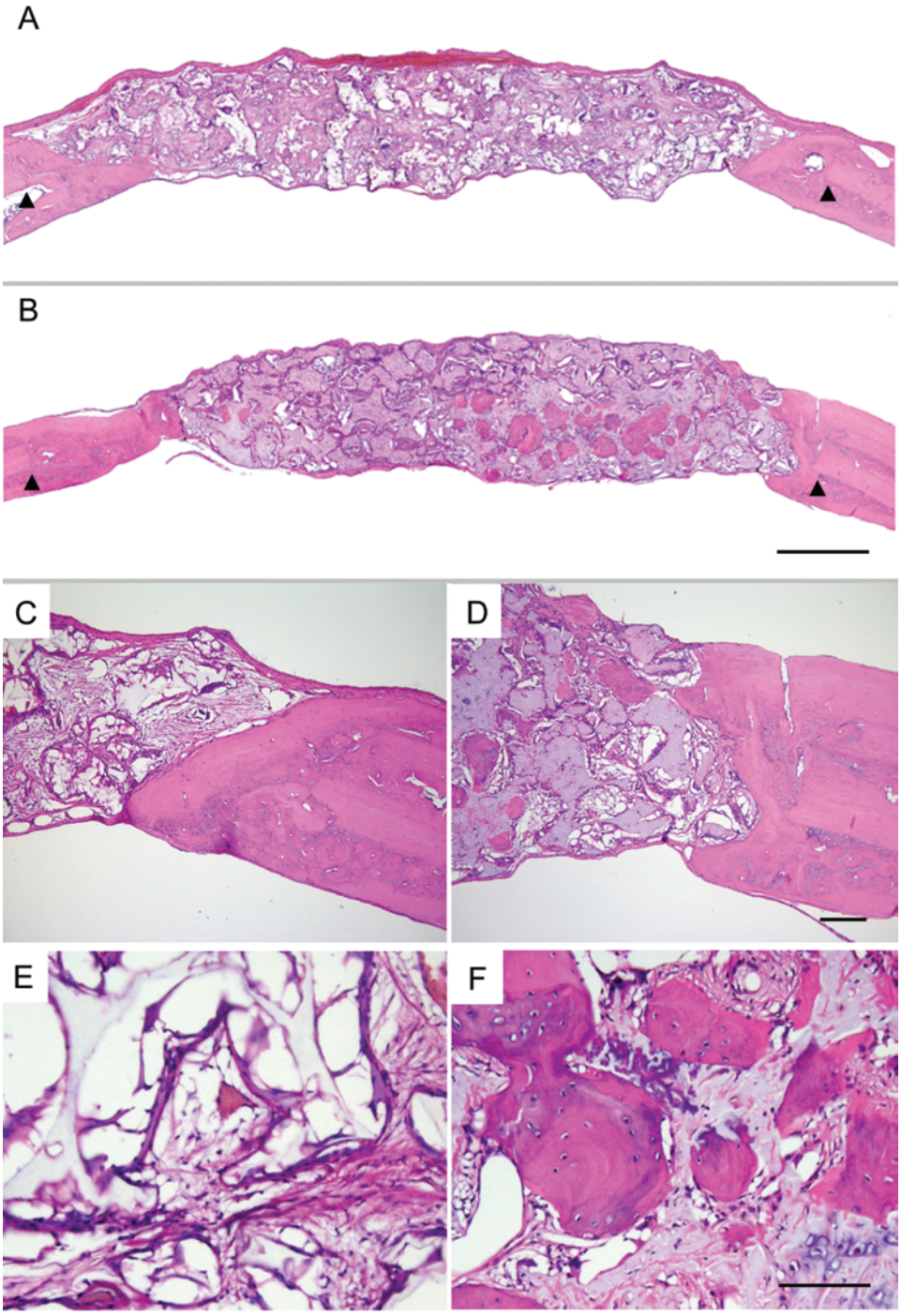

FIG. 3. Histological images of H&E-stained solid-walled scaffolds (**A, C, E**) and nanofibrous scaffolds (**B, D, F**) implanted in calvarial defects for 8 weeks. Arrowheads mark the site of original defects (**A, B**). Peripheral parts (**C, D**) and central parts (**E, F**) of the defects are shown. Original magnification: (**A, B**), 20×; (**C, D**), 100×; (**E, F**), 200×. Bar length: (**A, B**), 1 mm; (**C, D**), 100 μm; (**E, F**), 100 μm. Representative images are presented. Color images available online at www.liebertonline.com/ten.

confirmed by all measurements: reconstructed micro-CTs and histological analyses by von Kossa and H&E stains (Figs. 1A, 2, and 3). In solid-walled scaffolds new bone formation only occurred in the periphery of the disk-shaped scaffolds. In contrast, in the nanofibrous scaffolds new bone formation was observed both in the center and in the periphery. In the central area of nanofibrous scaffolds, the new bone nodules were more frequently observed on the dura mater side than on the pericranium side, and the new bone tissue was rich in cells (appearing as immature bone) and formed in the shape of globules in the pores of the scaffolds. There was not a significant difference in the amount and pattern of bone formation in the peripheral areas between the two types of scaffolds; new bone tissues were formed in linear apposition to adjacent bone, appearing more mature with a low cell density.

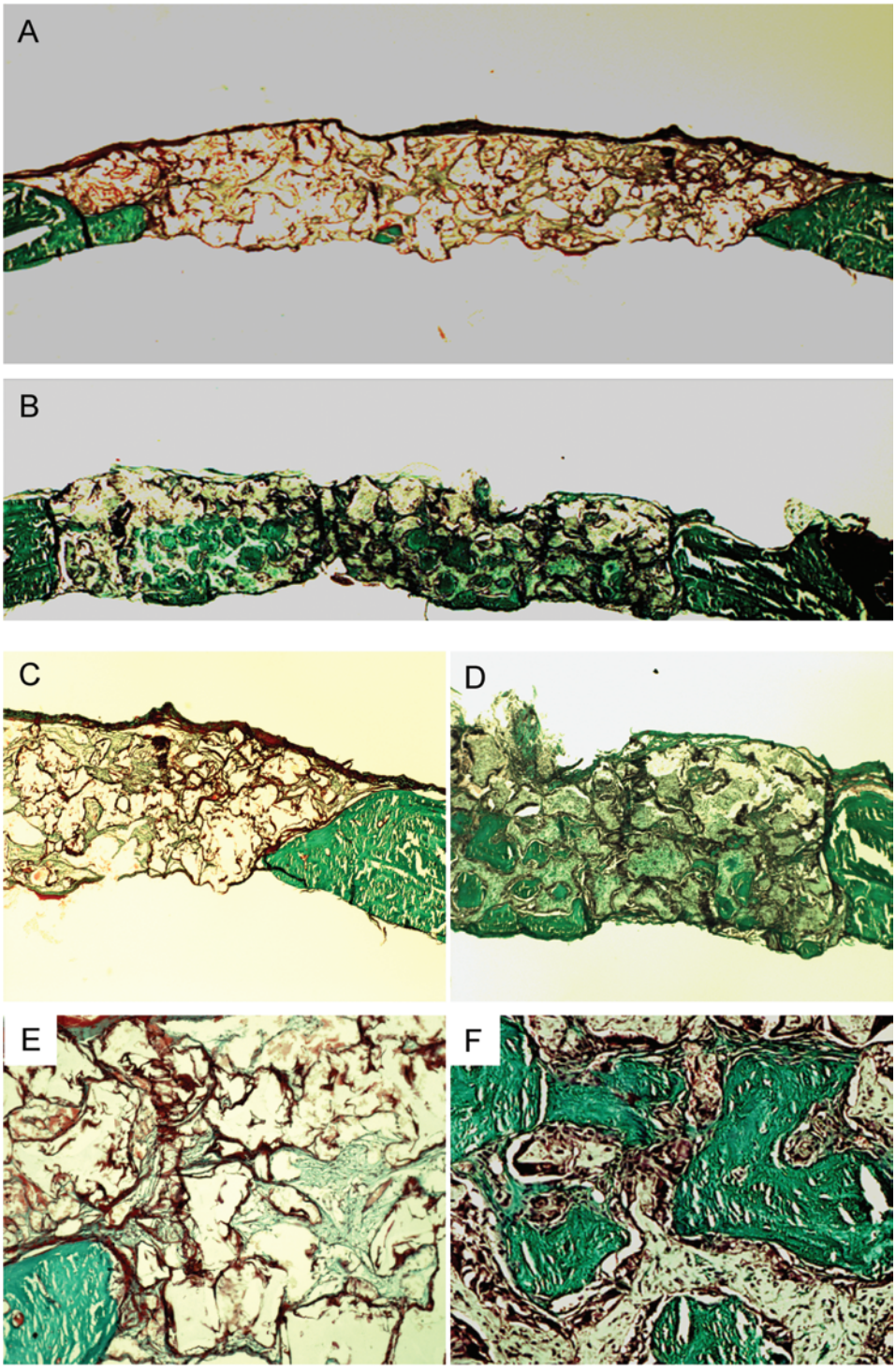

FIG. 4. Histological images by Goldner's Trichrome staining of solid-walled (**A**, **C**, **E**) and nanofibrous scaffolds (**B**, **D**, **F**) implanted in calvarial defects for 8 weeks. Collagens are stained in green color. Overall views (**A, B**), peripheral parts (**C, D**), and central parts (**E, F**) of the defects are shown. Original magnification: (**A, B**), 20×; (**C, D**), 100×; (**E, F**), 200×. Bar length: (**A, B**), 1 mm; (**C, D**), 100 μm; (**E, F**), 100 μm. Representative images are presented. Color images available online at www.liebertonline.com/ten.

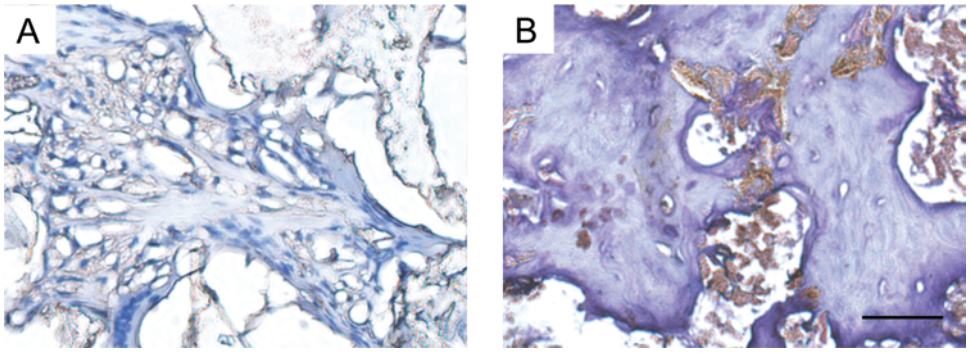

FIG. 5. Immunostaining for Runx2 protein in solid-walled scaffolds (**A**) and nanofibrous scaffolds (**B**) implanted in calvarial defects for 4 weeks. After immunostaining (dark brown), the sections were counterstained with hematoxylin. Original magnification, 200×. Bar length, 50 μm. Representative images are presented. Color images available online at www.liebertonline.com/ten.

Osteoblast phenotypes

The collagen formation within the implanted scaffolds was examined using Goldner's trichrome staining. As shown in Figure 4, green-stained dense collagen matrix was observed in nanofibrous scaffolds, especially inside the pores of the scaffolds, where von Kossa staining was also positive. The solid-walled scaffolds were low in collagen (green) although cells (stained in red) were not rare. The cells in the scaffolds were examined for osteoblastic differentiation through immunostaining for the Runx2 (early osteogenic marker) and BSP (late osteogenic marker). The cells in nanofibrous scaffolds strongly stained (dark brown) for Runx2 and BSP, especially in cells around the ossicles (Figs. 5 and 6). The solid-walled scaffolds, however, had very weak stains. These results suggest that the cells recruited to nanofibrous scaffolds differentiated to osteoblasts responsible for collagen synthesis and mineralized bone formation.

Discussion

This *in vivo* study was to determine whether the nanofibrous architecture of 3D porous scaffolds is suitable for use in bone regeneration. We compared the bone regenerative properties of nanofibrous 3D scaffolds with those of solid-walled 3D scaffolds implanted in a rat critical-size calvarial bone defect. Both types of scaffolds were made from the same polymer (PLLA) and had the same macropore structure (interconnected spherical pores). Their porosities and pore sizes were also similar. The difference was in the wall architecture of the macropores, i.e., either nanofibrous or solid-walled (no fibrous feature). In this study, the scaffolds without cells were implanted in the defects to highlight the effect of scaffolding structure on bone regeneration by host cells. The results demonstrate that the nanofibrous structure of scaffolds enhances osteoblast differentiation, collagen matrix deposition, and mineralized bone formation, as confirmed by immunostaining for Runx2 and BSP, Goldner's trichrome staining for collagen, and von Kossa staining and micro-CT measurement for mineral contents. The cells that differentiated to bone-forming osteoblasts were most likely derived from tissues surrounding the defects: the dura mater, the pericranium, and the bone tissues. These three tissue types have been reported to contain cells responsible for bone formation in similar defects.[20] The most notable difference between the nanofibrous and the solid-walled scaffolds was in the location where bone formation occurred. The central part of nanofibrous scaffolds, but not that of solid-walled scaffolds, contained numerous globular ossicles. The cells responsible for bone formation in the central part should have come from dura mater or pericranium, which need a cue to differentiate into functional osteoblasts. We previously found that synthetic nanofibers enhanced osteoblast differentiation and mineralization *in vitro*.[16] We showed in this *in vivo* study that the cells in nanofibrous scaffolds were strongly immunostained for Runx2 and BSP, and that bone formation in the nanofibrous scaffolds was at a much higher level than that in the solid-walled scaffolds. These results indicate that nanofibrous scaffolds provide a better environment for osteoblastic differentiation *in vivo* as well.

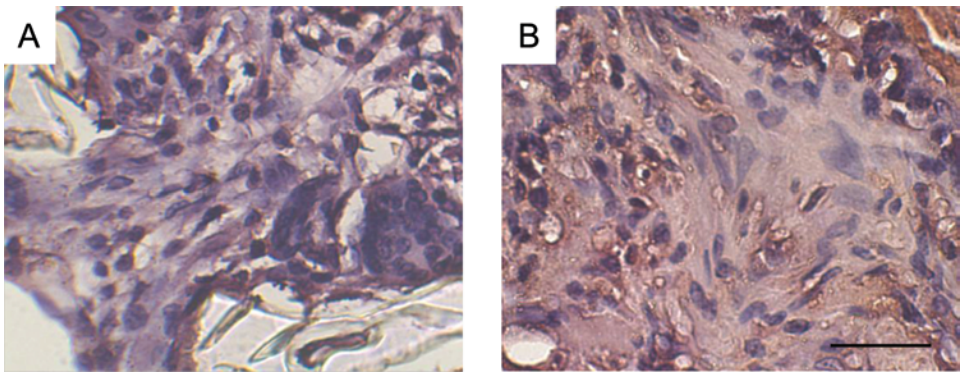

FIG. 6. Immunostaining for BSP in solid-walled scaffolds (**A**) and nanofibrous scaffolds (**B**) implanted in calvarial defects for 4 weeks. After immunostaining (dark brown), the sections were counterstained with hematoxylin. Original magnification, 200×. Bar length, 50 μm. Representative images are presented. Color images available online at www.liebertonline.com/ten.

The nanofibrous scaffolds were developed to mimic the fibrous morphology of type I collagen, a major component of bone ECM that is known to affect osteoblast behavior. Cells grown on collagen exhibit an earlier and enhanced osteoblast phenotype.[21] Collagen also positively mediates biomineralization.[22] It was recently reported that mineral was deposited by Runx2-expressing fibroblasts seeded on collagen, but not on smooth polymer scaffolds.[23] Previously, we showed that synthetic nanofibers enhanced the adsorption of adhesion proteins (likely due partially to the larger surface area[24] of and partially to their preferential interaction[15] with the nanofibrous scaffold) from the serum in culture medium and enhanced the expression of a few integrins, which may have contributed to the cell signaling.[15,16] We also found that the osteoblastic differentiation of cells on nanofibrous scaffolds was enhanced by the nanofibrous geometry (compared to solid-walled scaffolds) rather than a collagen-mimicking chemistry (gelatin surface coating), and the enhanced BSP gene expression was associated with the RhoA-ROCK signaling pathway.[18]

We would like to mention the possible contributions of local mass transport conditions. Although the overall pore sizes and porosities were essentially the same for the two types of scaffolds as discussed earlier, the local mass transport conditions for cells in contact with the nanofibrous and solid-walled pores might likely be different. The nanofibrous pore walls might allow for improved nutrient/oxygen supply to and metabolic waste removal from the attached cells. The *in vitro* faster degradation of nanofibrous scaffolds does not seem fast enough to result in significant scaffold macropore change within the experimental time frame.[24] However, the *in vivo* degradation properties of the two types of PLLA scaffolds have not been carefully compared to rule out their possible effect.

In any case, this study confirmed that synthetic polymers with a nanofibrous morphology could promote osteoblast differentiation and bone formation in an *in vivo* model. Taken together, the synthetic nanofibrous PLLA scaffolds, by mimicking the geometrical features of collagen fibers, enhance their capacity to facilitate both *in vitro* and *in vivo* osteoblast differentiation and bone formation.

Conclusion

Nanofibrous scaffolds, mimicking the fibrous morphology of type I collagen, supported bone formation when the scaffolds were implanted in a rat critical-size calvarial defect, while solid-walled scaffolds resulted in very limited amounts of bone formation in only the peripheral regions. More collagen was synthesized in nanofibrous scaffolds than in solid-walled scaffolds. Cells in nanofibrous scaffolds expressed higher levels of Runx2 and BSP, especially near the newly formed ossicles. These findings suggest that nanofibrous scaffolds promote osteoblast differentiation and bone formation, and are excellent scaffolds for bone tissue engineering.

Acknowledgments

The authors wish to acknowledge the financial support from the Basic Research Program of the Korea Science & Engineering Foundation (R01-2005-000-106650 to K.M.W.), and the NIH-NIDCR&NIGMS of the United States (DE15384&17689 and GM75840 to P.X.M.).

Disclosure Statement

No competing financial interests exist.

References

1. Ma, P.X. Tissue engineering. In: Kroschwitz, J.I., ed. Encyclopedia of Polymer Science and Technology. Hoboken, NJ: John Wiley & Sons, Inc., 2005, pp. 261–291 (www.mrw.interscience.wiley.com/epst).
2. Ma, P.X. Biomimetic materials for tissue engineering. Adv Drug Deliv Rev **60,** 184, 2008.
3. Ma, P.X., and Zhang, R. Synthetic nano-scale fibrous extracellular matrix. J Biomed Mater Res **46,** 60, 1999.
4. Zhang, R., and Ma, P.X. Synthetic nano-fibrillar extracellular matrices with predesigned macroporous architectures. J Biomed Mater Res **52,** 430, 2000.
5. Smith, L.A., and Ma, P.X. Nano-fibrous scaffolds for tissue engineering. Colloids Surf B Biointerfaces **39,** 125, 2004.
6. Li, W.J., Laurencin, C.T., Caterson, E.J., Tuan, R.S., and Ko, F.K. Electrospun nanofibrous structure: a novel scaffold for tissue engineering. J Biomed Mater Res **60,** 613, 2002.
7. Wnek, G.E., Carr, M.E., Simpson, D.G., and Bowlin, G.L. Electrospinning of nanofiber fibrinogen structures. Nano Lett **3,** 213, 2003.
8. Yoshimoto, H., Shin, Y.M., Terai, H., and Vacanti, J.P. A biodegradable nanofiber scaffold by electrospinning and its potential for bone tissue engineering. Biomaterials **24,** 2077, 2003.
9. Luo, Z., Zhao, X., and Zhang, S. Self-organization of a chiral D-EAK16 designer peptide into a 3D nanofiber scaffold. Macromol Biosci **8,** 785, 2008.
10. Beniash, E., Hartgerink, J.D., Storrie, H., Stendahl, J.C., and Stupp, S.I. Self-assembling peptide amphiphile nanofiber matrices for cell entrapment. Acta Biomater **1,** 387, 2005.
11. Chen, V.J., and Ma, P.X. Nano-fibrous poly(L-lactic acid) scaffolds with interconnected spherical macropores. Biomaterials **25,** 2065, 2004.
12. Wei, G., and Ma, P.X. Macroporous and nanofibrous polymer scaffolds and polymer/bone-like apatite composite scaffolds generated by sugar spheres. J Biomed Mater Res A **78,** 306, 2006.
13. Wei, G., Jin, Q., Giannobile, W.V., and Ma, P.X. The enhancement of osteogenesis by nano-fibrous scaffolds incorporating rhBMP-7 nanospheres. Biomaterials **28,** 2087, 2007.
14. Chen, V.J., Smith, L.A., and Ma, P.X. Bone regeneration on computer-designed nano-fibrous scaffolds. Biomaterials **27,** 3973, 2006.
15. Woo, K.M., Chen, V.J., and Ma, P.X. Nano-fibrous scaffolding architecture selectively enhances protein adsorption contributing to cell attachment. J Biomed Mater Res **67A,** 531, 2003.
16. Woo, K.M., Jun, J.H., Chen, V.J., Seo, J., Baek, J.H., Ryoo, H.M., Kim, G.S., Somerman, M.J., and Ma, P.X. Nano-fibrous scaffolding promotes osteoblast differentiation and biomineralization. Biomaterials **28,** 335, 2007.
17. Ma, P.X., and Choi, J.W. Biodegradable polymer scaffolds with well-defined interconnected spherical pore network. Tissue Eng **7,** 23, 2001.
18. Hu, J., Liu, X., and Ma, P.X. Induction of osteoblast differentiation phenotype on poly(L-lactic acid) nanofibrous matrix. Biomaterials **29,** 3815, 2008.
19. Hollinger, J.O., and Kleinschmidt, J.C. The critical size defect as an experimental model to test bone repair materials. J Craniofac Surg **1,** 60, 1990.

20. Gosain, A.K., Santoro, T.D., Song, L.S., Capel, C.C., Sudhakar, P.V., and Matloub, H.S. Osteogenesis in calvarial defects: contribution of the dura, the pericranium, and the surrounding bone in adult versus infant animals. Plast Reconstr Surg **112,** 515, 2003.
21. Lynch, M.P., Stein, J.L., Stein, G.S., and Lian, J.B. The influence of type I collagen on the development and maintenance of the osteoblast phenotype in primary and passaged rat calvarial osteoblasts: modification of expression of genes supporting cell growth, adhesion, and extracellular matrix mineralization. Exp Cell Res **216,** 35, 1995.
22. Bonucci, E. Role of collagen fibrils in calcification. In: Bonucci, E., ed. Calcification in Biologic Systems. Boca Raton, FL: CRC Press, 1992, pp. 19–39.
23. Phillips, J.E., Hutmacher, D.W., Guldberg, R.E., and Garcia, A.J. Mineralization capacity of Runx2/Cbfa1-genetically engineered fibroblasts is scaffold dependent. Biomaterials **27,** 5535, 2006.
24. Chen, V.J., and Ma, P.X. The effect of surface area on the degradation rate of nano-fibrous poly(L-lactic acid) foams. Biomaterials **27,** 3708, 2006.

Address correspondence to:
Peter X. Ma, Ph.D.
Department of Biologic and Materials Sciences
The University of Michigan
1011 North University Ave., *Room 2211*
Ann Arbor, MI 48109-1078

E-mail: mapx@umich.edu

Received: July 26, 2008
Accepted: December 12, 2008
Online Publication Date: April 3, 2009